NANO LETTERS

Letter

pubs.acs.org/NanoLett

Triboelectric-Generator-Driven Pulse Electrodeposition for Micropatterning

Guang Zhu, Caofeng Pan, Wenxi Guo, Chih-Yen Chen, Yusheng Zhou, Ruomeng Yu, and Zhong Lin Wang*

School of Materials Science and Engineering, Georgia Institute of Technology, Atlanta, Georgia 30332-0245, United States

Supporting Information

ABSTRACT: By converting ambient energy into electricity, energy harvesting is capable of at least offsetting, or even replacing, the reliance of small portable electronics on traditional power supplies, such as batteries. Here we demonstrate a novel and simple generator with extremely low cost for efficiently harvesting mechanical energy that is typically present in the form of vibrations and random displacements/deformation. Owing to the coupling of contact charging and electrostatic induction, electric generation was achieved with a cycled process of contact and separation between two polymer films. A detailed theory is developed for understanding the proposed mechanism. The instantaneous electric power density reached as high as 31.2 mW/cm^3 at a maximum open circuit voltage of 110 V. Furthermore, the generator was successfully used without electric storage as a direct power source for pulse electrodeposition (PED) of micro/nanocrystalline silver structure. The cathodic current efficiency reached up to 86.6%. Not only does this work present a new type of generator that is featured by simple fabrication, large electric output, excellent robustness, and extremely low cost, but also extends the application of energy-harvesting technology to the field of electrochemistry with further utilizations including, but not limited to, pollutant degradation, corrosion protection, and water splitting.

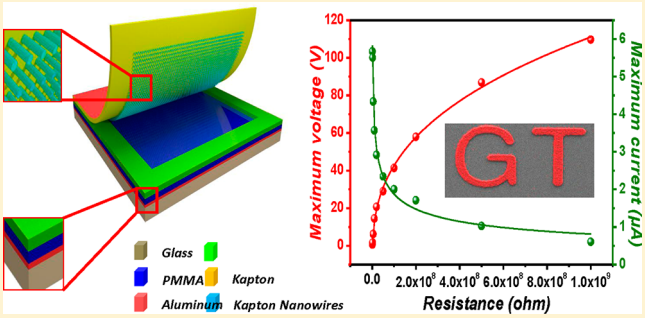

KEYWORDS: *Triboelectric-generator, electrodeposition, self-powering*

By converting ambient energy into electricity, energy harvesting is capable of at least offsetting, or even replacing, the reliance of small portable electronics on traditional power supplies, such as batteries.[1,2] Especially when long-term operation of a large number of electronic devices in dispersed locations is required, energy harvesting distinguishes itself from batteries and hardwire power owing to inherent advantages, such as outstanding longevity, little maintenance, and minimal disposal/contamination. Despite of these benefits, superior performance, miniaturized size and competitive prices are still to be sought after in order for the energy harvesting technology becoming prevalent. Here we demonstrate a novel and simple generator with extremely low cost for efficiently harvesting mechanical energy that is typically present in the form of vibrations and random displacements/deformation. Owing to the coupling of contact charging and electrostatic induction,[3,4] electric generation was achieved with a cycled process of contact and separation between two polymer films. The instantaneous electric power density reached as high as 31.2 mW/cm^3. Furthermore, the generator was successfully used without electric storage as a direct power source for pulse electrodeposition (PED) of micro/nanocrystalline silver structure. The cathodic current efficiency reached up to 86.6%. Not only does this work present a new type of generator that is featured by simple fabrication, large electric output, excellent robustness, and extremely low cost, but also extends the application of energy-harvesting technology to the field of electrochemistry with further utilizations including, but not limited to, pollutant degradation, corrosion protection, and water splitting.

Harvesting mechanical energy has been achieved by electromagnetic,[5,6] piezoelectric[7,8] and electrostatic[9,10] mechanisms. However, widespread usage of these techniques is likely shadowed by possible limitations, such as structure complexity,[11] fabrication of high-quality materials,[12] and reliance on external power source.[11] Here, our new type of generator can properly address all of these issues. Schemed in Figure 1, it has a multilayer structure. Between two polymer layers, a cavity is formed, which is sustained by a spacer designed for the charge generation and separation processes. The fabrication process in detail is discussed in Methods.

The operating principle of the generator can be described by the coupling of contact charging and electrostatic induction. Respectively, Figure 2a,b depicts electric output of open-circuit voltage and short-circuit current. At original state, no charge is generated or inducted with no electric potential difference

Received: July 11, 2012
Revised: August 10, 2012

   dx.doi.org/10.1021/nl302560k | *Nano Lett.* XXXX, XXX, XXX−XXX

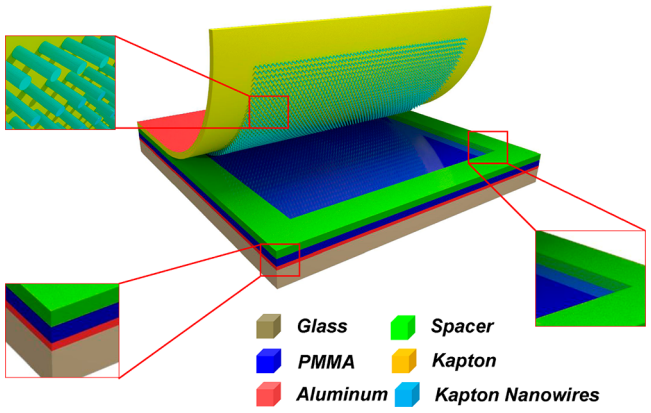

Figure 1. Sketch of the generator's structure and materials selection. The polymer nanowires (PNWs) are depicted with a different color from the substrate for clear visualization even though they are the same material.

(EPD) between the two electrodes (Figure 2a I). With an externally introduced displacement, the two polymers are brought into contact with each other. Surface charge transfer then takes place at the contact area due to triboelectric effect.[13−15] According to the triboelectric series,[16] that is, a list of materials based on their tendency to gain or lose charges, electrons are injected from poly(methyl methacrylate) (PMMA) into Kapton, resulting in net negative charges at the Kapton surface and net positive charges at the PMMA surface. It is worth noting that the insulating property of the polymers allows a long-time retention of triboelectric charges for hours or even days.[17] Since they are only confined on the surface,[18,19] charges with opposite signs coincide at almost the same plane, generating practically no EPD between the two electrodes (Figure 2a II).

As the generator starts to be released, the Kapton film intends to revert back to its original position due to its own resilience. Once the two polymers separate, an EPD is then established between the two electrodes (Figure 2a III). If we define electric potential of the bottom electrode (U_{BE}) to be zero, electric potential of the top electrode (U_{TE}) can be calculated by

$$U_{TE} = -\frac{\sigma d'}{\varepsilon_0} \quad (1)$$

where σ is the triboelectric charge density, ε_0 is the vacuum permittivty, and d' is the interlayer distance at a given state (Supporting Information).

Here, we define a forward connection for measurement as a configuration with positive end of the electrometer connected to the bottom electrode (BE). All electric measurements in this paper are based on the forward connection unless otherwise stated. Therefore, as the generator is being released, V_{oc} keeps increasing until reaching the maximum value when the Kapton film fully reverts to the original position (Figure 2a IV,V). Such a signal will remain constant provided that the input impedance of the electrometer is infinitely large.

If pressing is immediately followed, the EPD starts diminishing as the two polymer layers get closer to each other. As a result, V_{oc} drops from the maximum value to zero when a full contact is made again between the two polymers (Figure 2a II,VI).

If the two electrodes are shorted, any established EPD shown in eq 1 as the two polymers separate drives electrons from the top electrode (TE) to the BE (Figure 2b III), resulting in an instantaneous positive current during the releasing process

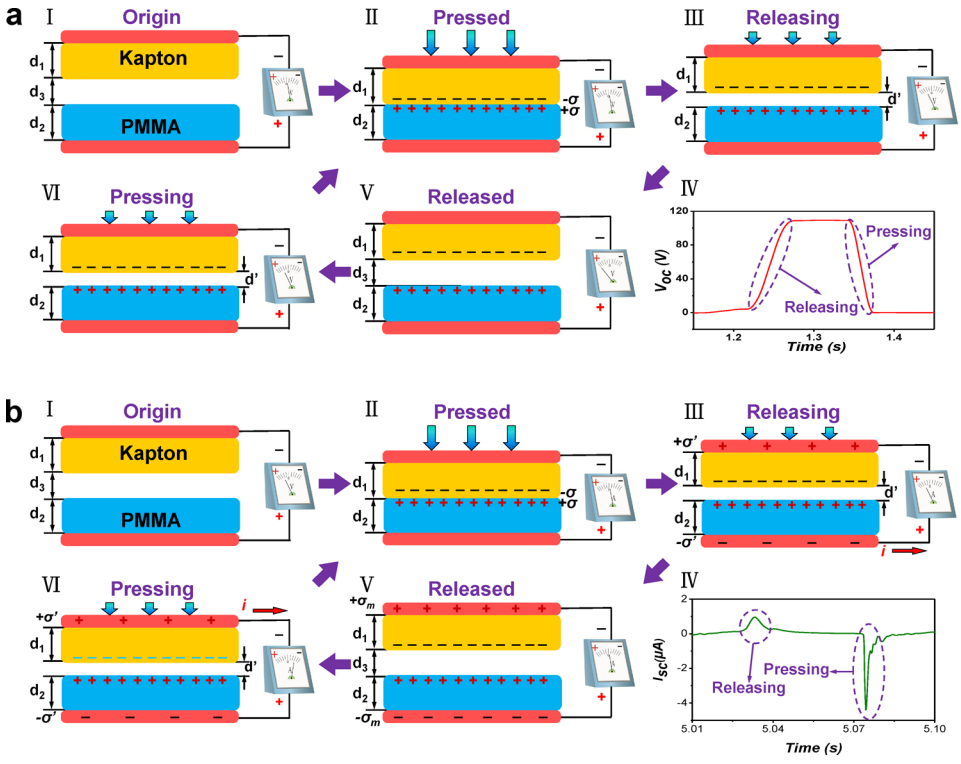

Figure 2. Sketches that illustrate the operating principle of the generator. (a) Open-circuit condition. (b) Short-circuit condition. The polymer nanowires and the spacer are not shown for the purpose of simplification.

dx.doi.org/10.1021/nl302560k | Nano Lett. XXXX, XXX, XXX−XXX

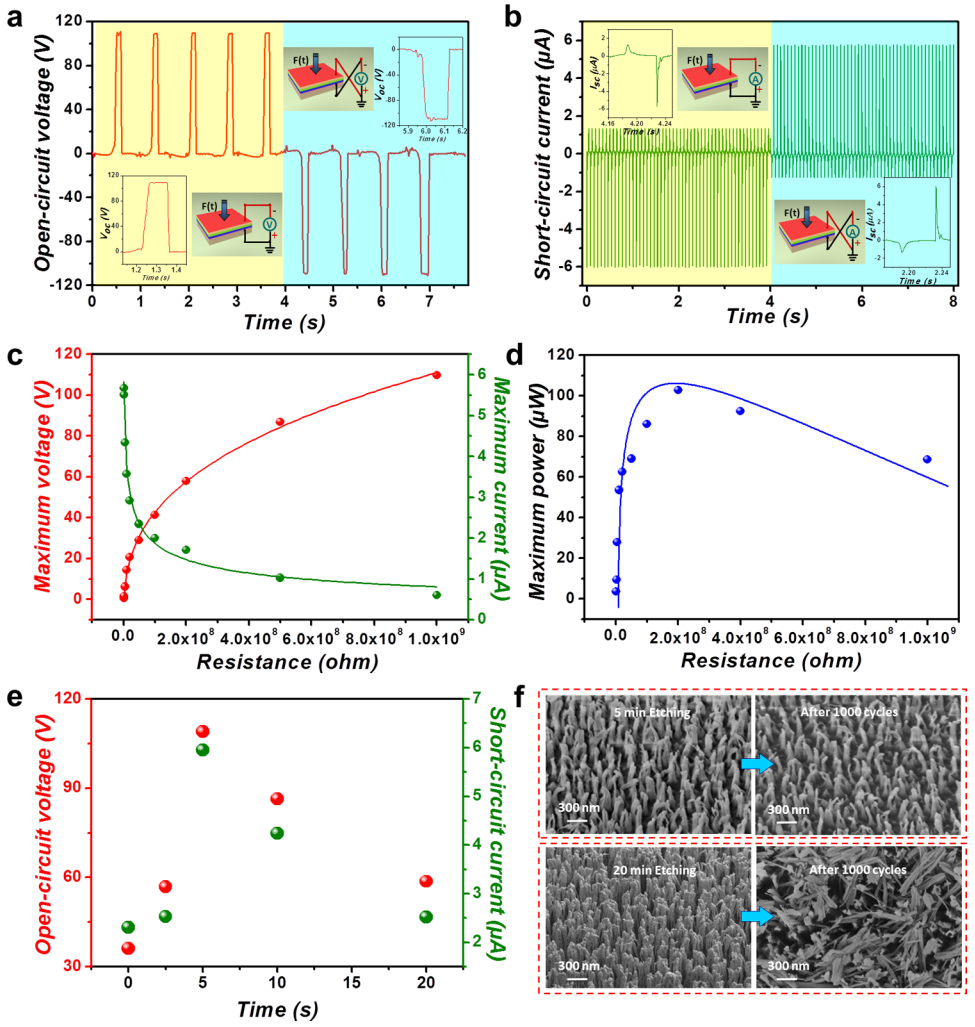

Figure 3. Investigation on the performance of the generator. (a) Open-circuit voltage with forward connection on the left half (bottom-left insets) and reverse connection on the right half (upper-right insets). (b) Short-circuit current with forward connection on the left half (upper-left insets) and reverse connection on the right half (bottom-right insets). (c) Electric voltage (left axis) and current (right axis) as a function of the load resistance. The dots are experimentally measured values, while the lines are fitted results. (d) Instantaneous electric power as a function of the load resistance. The dots are experimentally measured values, while the line is a fitted result. (e) The effect of time for etching polymer nanowires on open-circuit voltage (left axis) and short-circuit current (right axis). (f) SEM images of the PNWs before (left pairs) and after (right pairs) the generator operates for 1000 cycles to explain why PNWs with proper length (top pairs) contribute to much more enhanced electric output than do excessively long PNWs (bottom pairs).

(Figure 2b IV). The net effect is that inducted charges accumulate with positive sign on the TE and negative sign on the BE (Figure 2 V). The inducted charge density (σ') when the generator is fully released can be expressed as below

$$\sigma' = \frac{\sigma d' \varepsilon_{rk} \varepsilon_{rp}}{d_1 \varepsilon_{rp} + d' \varepsilon_{rk} \varepsilon_{rp} + d_2 \varepsilon_{rk}} \quad (2)$$

where ε_{rk}, and ε_{rp} are the relative permittivity of Kapton and PMMA, respectively, and d_1 and d_2 are the thickness of the Kapton film and the PMMA layer, respectively (Supporting Information). The maximum value of σ'_{max} is obtained by substituting d_3, the spacer height, for d' in the equation above.

Once the generator is pressed again, reduction of the interlayer distance would make the TE possess a higher electric potential than the BE. As a consequence, electrons are driven from the BE back to the TE, reducing the amount of inducted charges (Figure 2b VI). This process corresponds to an instantaneous negative current (Figure 2b IV). When the two polymers are in contact again, all inducted charges are neutralized (Figure 2b II).

As triggered by a vibration source with controlled frequency and amplitude, the generator produced an open-circuit voltage (Figure 3a) and a short-circuit current (Figure 3b) as predicted in the above analytical model. Electric output with opposite sign was obtained by switching the polarity for electric measurement. The peak value of the V_{oc} and I_{sc} were up to 110 V and 6 μA, respectively. Substituting the experimentally determined V_{oc} into eq 1, we obtained a theoretical triboelectric charge density

$$\sigma = \frac{V_{oc}\varepsilon_0}{d_3} = 97.39\ \mu\text{C m}^{-2} \quad (3)$$

Then based on eq 2, the maximum inducted charge density (σ'_{max}) was theoretically calculated to be

dx.doi.org/10.1021/nl302560k | Nano Lett. XXXX, XXX, XXX−XXX

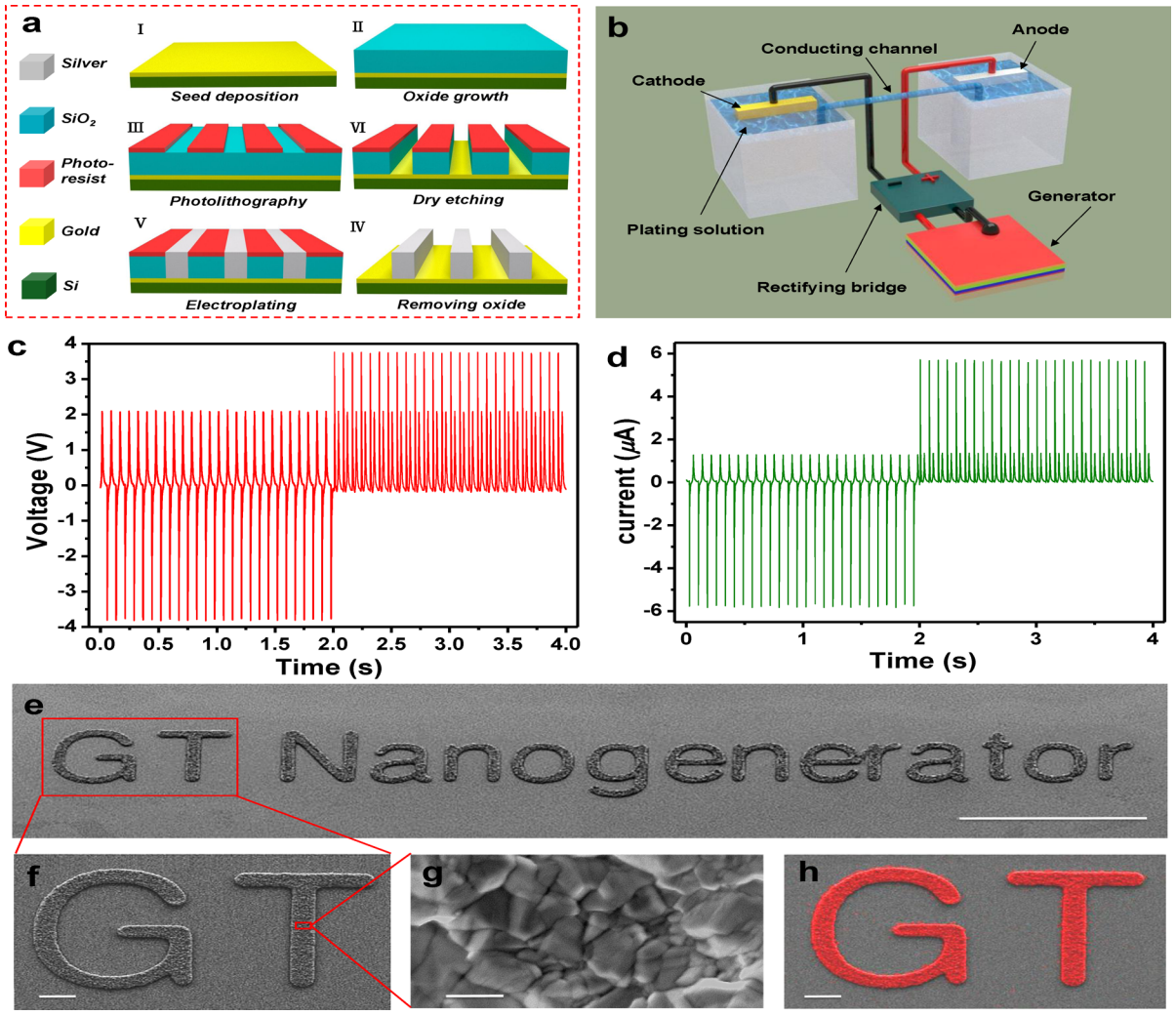

Figure 4. Pulse electrodeposition of silver microstructure by using the generator as a power source. (a) Sketches that illustrate the process for fabricating the silver structure. (b) Setup for the pulse electrodeposition. (c) Electric voltage between the cathode and the anode with (right half) and without (left half) rectification. (d) Electric current through the plating solution with (right half) and without (left half) rectification. (e) SEM image of the deposit showing clearly and uniformly defined structure (tilted angle of 45°). The scale bar is 100 μm. (f) SEM image of the deposit with enlarged view (tilted angle of 45°). The scale bar is 5 μm. (g) SEM image of the densely packed grain structure. The scale bar is 200 nm. (h) EDS mapping which confirms that the deposit is silver. The red color represents silver spacial distribution. The scale bar is 5 μm.

$$\sigma'_{\max} = \frac{\sigma d_3 \varepsilon_{rk} \varepsilon_{rp}}{d_1 \varepsilon_{rp} + d_3 \varepsilon_{rk} \varepsilon_{rp} + d_2 \varepsilon_{rk}} = 73.72\ \mu\text{C m}^{-2} \quad (4)$$

Therefore, electrons are pumped back and forth between the two electrodes as a result of contact charging and electrostatic induction. For one cycle of contacting−sliding−separating, the integration of current over time for releasing has the same value as that for pressing, indicating that equal amount of electrons flow in the opposite direction (Supporting Information Figure S1). It is observed that the current peak corresponding to releasing has a smaller magnitude but lasts longer than that for pressing (insets in Figure 3b). Such an observation can be explained by the fact that pressing is caused by the external vibration source while it is the resilience of the Kapton film that leads to releasing. Therefore, it is very likely that releasing corresponds to a slower process and thus a smaller but wider current signal. Having the maximum inducted charge (Q'), the corresponding charge density was obtained as

$$\sigma'_{\max} = \frac{Q'}{S} = 87.23\ \mu\text{C m}^{-2} \quad (5)$$

where S is the electrode area that is the same as the device area (Supporting Information Table S1.).

The experimental result in eq 5 is only slightly larger than the theoretically calculated one in eq 4, indicating that the model is fairly valid for explaining the working principle. The difference is probably attributed to simplifications made in the model and errors that may occur in the measurement (Supporting Information).

External load matching for the generator has also been investigated. With an increase in the load resistance, the maximum current decreases due to ohmic loss, while the maximum voltage across the load has an opposite trend (Figure 3c). Accordingly, the electric power exhibits an instantaneous peak value of 110 μW (Figure 3d), which is in correspondence to a power density of 31.2 mW/cm^3. The measurement results reveal that the generator is particularly efficient provided that the load has a resistance on the order of megaohms.

dx.doi.org/10.1021/nl302560k | Nano Lett. XXXX, XXX, XXX−XXX

Our demonstrated generator features simple fabrication/implementation, low cost, and strong performance. Previously reported electrostatic generators usually required precharging by external power source in order to introduce electrostatic force.[9] On the contrary, our generator is self-charged with triboelectric charges instantly generated upon contact. Besides, the fabrication processing is highly straightforward with neither material synthesis nor micromachining. The selection of materials is cost-oriented. Extremely low cost for fabrication and materials is thus anticipated, which is likely to be further reduced for mass production.

The calculated triboelectric charge density shown in eq 3 is substantially larger than previous reported.[14,15] Moreover, the generator largely outperforms recent demonstrations based on electrostatic mechanism.[9,10] Several factors may be attributed to this largely enhanced performance. The first one is appropriate selection of materials. Substantial polarity difference exists between Kapton and PMMA according to the triboelectric series, leading to very effective charge transfer upon contact. In addition, the spacer structure plays an important role. The spacer's height not only relates to V_{oc} as indicated in eq 1, but also affects I_{sc} according to eq 4. Without the spacer, only very little electric output could be detected (Supporting Information). Furthermore, surface morphology modification is another key factor. Here, selective dry etching was applied on the Kapton surface to create vertically aligned polymer NWs with longer etching corresponding to larger aspect ratio of the NWs (Supporting Information Figure S2). Enhanced surface roughness as a result of the NWs is expected to introduce additional friction as the two polymers are brought into contact (Supporting Information Figure S3a). Such frictional movement is likely to generate more triboelectric charges[13] and thus enhanced electric output is achieved. However, experimental observation shows that the electric output substantially drops with excessive etching time (Figure 3e). For NWs with proper length (hundreds of nanometers), the elastic property ensures retained orientation and morphology of the NWs even after numerous contacts (Figure 3f and Supporting Information Figure S3a). For overly long NWs, strain generated at the root is likely to exceed the elastic limit of the polymer material, resulting in permanent deformation (Figure 3f and Supporting Information Figure S3b). As a result, they are no longer able to introduce effective friction, which explains the less enhanced electric output.

As a demonstration of applications, we successfully achieved cyanide-free PED of silver structure on micrometer scale by using the generator as a power source. The resultant electroplated silver material has excellent uniformity, density, and surface smoothness, which is suitable for either thin film deposition or structure fabrication.

The process of creating a desired silver structure is schemed in Figure 4a. We deposited a silicon substrate with gold, followed by growth of silicon dioxide as a mask layer. High work function of gold ensures that it only acts as a seed material but not reacts with plating solution. Standard photolithography was conducted to generate the desired pattern on the oxide, which was then etched through so that gold surface with the defined pattern was exposed. Subsequently, electroplating was performed with the gold surface as the cathode and silver metal as the sacrificial anode. Finally, the oxide layer was removed by isotropic wet etching.

The setup for electroplating is schemed in Figure 4b with preparation of the plating solution discussed in Methods and Supporting Information. Different from conventional electroplating in which cathode and anode are bathed in the same container, our setup has separated baths that are connected by a long and thin hollow channel filled with the plating solution. As previously discussed, electric voltage delivered by the generator across an external load is a function of resistance (Figure 3c). The purpose of adding the conducting channel is to increase the resistance of the solution so that a sufficient voltage between the cathode and the anode can be established for effective electroplating.

The voltage across the two electrodes and the current passing through the solution are demonstrated in Figure 4c,d, respectively. The alternating electric output can be rectified by a full-wave bridge, resulting in bursts of pulses that are suitable for PED. Compared to DC power source, the pulsed waveform can significantly raises the limiting current density by replenishing metal ions in the diffusion layer.[20] Besides, metal ions are able to migrate to depleted regions with high current density, such as edges and corners.[21] Therefore, with improved mass transport and more evenly distributed ions, not only higher plating rate but also better coating quality is expected to be achieved.[20] By modifying pulse parameters, deposits with desired composition, morphology, porosity, and hydrogen content could be obtained.[22,23]

The waveform delivered by the generator is distinct from previously demonstrated waveforms. It provides pulses with constantly changing magnitude. Here, we have three independent variables, viz, (i) ON-time (T_{ON}), (ii) OFF-time (T_{OFF}) and (iii) total charge within a cycle (Q) (Supporting Information Figure S4). On the basis of these three variables, some characteristic pulse parameters can be calculated as below (Supporting Information)

$$\text{Duty cycle } (\gamma) = \frac{T_{ON}}{T_{cycle}} = \frac{(T_{ON1} + T_{ON2})}{(T_{ON} + T_{OFF})}100\% = 42.9\% \tag{8}$$

$$\begin{aligned}&\text{Average cathodic current density } (I_A)\\ &= \frac{Q}{ST_{cycle}}\\ &= \frac{\int_0^{T_{cycle}} I(t)\mathrm{d}t}{ST_{cycle}}\\ &= 0.38\ \text{A dm}^{-2}\end{aligned} \tag{9}$$

where S is the effective area of the work piece that is actually being deposited.

The SEM images of the electroplated silver structure are displayed by Figure 4e,f. The deposit protrudes from the surrounding surface. It is clearly and uniformly defined. Further zoomed-in view reveals that extremely fine grain size from 0.1 to 0.5 μm are densely packed (Figure 2g). The deposit is confirmed to be silver by EDS analysis results, as demonstrated in Figure 4h and Supporting Information Figure S5. The cathodic current efficiency was calculated to be 86.6% (Supporting Information). Further systematic investigations are still needed to understand how the specific waveform affects properties of the deposit.

In summary, we demonstrated a new type of self-charged generator for harvesting mechanical energy based on a coupled process of contact charging and electrostatic induction. The generator has the virtue of highly simple fabrication/

dx.doi.org/10.1021/nl302560k | Nano Lett. XXXX, XXX, XXX−XXX

implementation, strong performance, and extremely low cost, which properly address limitations of energy-harvesting technology. The instantaneous electric power density was up to 31.2 mW/cm^3. Moreover, it was applied as a pulsed power source for effectively electroplating uniform silver microstructure with fine grain size. The demonstrated cathodic current efficiency reached 86.6%. Our work not just only demonstrates a promising energy-harvesting technique but also greatly broadens the application of energy-harvesters.

Methods. *Fabrication of the Generator.* The fabrication process started with a square glass sheet, which was deposited with a thin layer of aluminum as the bottom electrode using electron beam evaporator. Then a thin layer of PMMA was spun-coated, followed by adding a spacer layer at the edges, leaving a square cavity at the center. One side of a Kapton film was deposited with a layer of aluminum as the top electrode, while the other side was dry-etched to create vertically aligned polymer nanowires (PNWs).[24] Then it was anchored on the spacer with the top electrode facing up. The spacer was made of insulating polymer with double-sided adhesive, keeping the Kapton film at a fixed distance away from the PMMA layer underneath.

Pulse Electrodeposition of Silver. Preparation of the plating solution is described as follows. In the first step, silver nitrate solution, sulfosalicylic acid solution, ammonium acetate solution, and potassium hydrate solution were prepared in separate containers. Then the silver nitrate solution was added into the potassium hydrate solution, forming dark-brown precipitate of silver hydroxide. Such a suspension was then added into the sulfosalicylic acid solution with strong agitation. After the precipitate disappears, the ammonium acetate solution was added. Finally, aqueous ammonia and DI water were applied to adjust pH and volume of the solution to desired levels, respectively. No additives, such as surfactant or brightening agent, were applied. The recipe for the solution is tabulated in the Supporting Information.

■ ASSOCIATED CONTENT

Supporting Information

Additional information, figures, and tables. This material is available free of charge via the Internet at http://pubs.acs.org.

■ AUTHOR INFORMATION

Corresponding Author

*E-mail: zlwang@gatech.edu.

Notes

The authors declare no competing financial interest.

■ ACKNOWLEDGMENTS

This research was supported by Research was supported by DARPA (HR0011-09-C-0142), Airforce, U.S. Department of Energy, Office of Basic Energy Sciences under Award DE-FG02-07ER46394, NSF (CMMI 0403671), and the Knowledge Innovation Program of the Chinese Academy of Sciences (Grant KJCX2-YW-M13).

■ REFERENCES

(1) Wang, Z. L. Self-powered nanogenerators and nanosystems. *Adv. Mater.* **2011**, *24*, 279−284.
(2) Wang, Z. L. Self-powered nanotech—Nanosize machines need still tinier power plants. *Sci. Am.* **2008**, *298*, 82−87.
(3) Fan, F. R.; Tian, Z. Q.; Wang, Z. L. Flexible triboelectric generator. *Nano Energy* **2012**, *1*, 328−334.
(4) Fan, F. R.; Lin, L.; Zhu, G.; Wu, W.; Zhang, R.; Wang, Z. L. Transparent Triboelectric nanogenerators and self-powered pressure sensors based on micropatterned plastic films. *Nano Lett.* **2012**, *12* (6), 3109−3114.
(5) Beeby, S. P.; Torah, R. N.; Tudor, M. J.; Jones, P. G.; Donnell, T. O.; Saha, C. R.; Roy, S. A micro electromagnetic generator for vibration energy harvesting. *J. Micromech. Microeng.* **2007**, *17*, 1257−1265.
(6) Saha, C. R.; Donnell, T. O.; Wang, N.; McCloskey, P. Electromagnetic generator for harvesting energy from human motion. *Sens. Actuators, A* **2008**, *147*, 248−253.
(7) Jeon, Y. B.; Sood, R.; Jeong, J.; Kim, S. MEMES power generator with transverse mode thin film PZT. *Sens. Actuators, A* **2005**, *122*, 16−22.
(8) Wang, Z. L.; Song, J. H. Piezoelectric nanogenerators based on zinc oxide nanowire arrays. *Science* **2006**, *312*, 242−246.
(9) Mitcheson, P. D.; Miao, P.; Stark, B. H.; Yeatman, E. M.; Holmes, A. S.; Green, T. C. MEMS electrostatic micropower generator for low frequency operation. *Sens. Actuators, A* **2004**, *115*, 523−529.
(10) Basset, P.; Galayko, D.; Paracha, A., M.; Marty, F.; Dudka, A.; Bourouina, T. A batch-fabricated and electrets-free silicon electrostatic vibration energy harvester. *J. Micromech. Microeng.* **2009**, *19*, 115025.
(11) Beeby, S. P.; Tudor, M. J.; White, N. M. Energy harvesting vibration sources for microsystems applications. *Meas. Sci. Technol.* **2006**, *17*, 175−195.
(12) Shen, D.; Park, J. H.; Noh, J. H.; Choe, S. Y.; Kim, S. H.; Kim, D. J. Micromachined PZT cantilever based on SOI structure for low frequency vibration energy harvesting. *Sens. Actuators, A* **2009**, *154*, 103−108.
(13) Castle, G. S. P. Contact charging between insulators. *J. Electrostat.* **1997**, *40−41*, 13−20.
(14) Nemeth, E.; Albrecht, V.; Schubert, G.; Simon, F. Polymer tribo-electric charging: dependence on thermodynamic surface properties and relative humidity. *J. Electrostat.* **2003**, *58*, 3−16.
(15) Lungu, M. Electrical separation of plastic materials using the triboelectric effect. *Miner. Eng.* **2004**, *17*, 69−75.
(16) Cross, J. A. *Electrostatics: Principles, Problems and Applications*; Adam Hilger: Bristol, 1987; Chapter 2.
(17) Saurenbach, F.; Wollmann, D.; Terris, B. D.; Diaz, A. F. Force microscopy of ion-containing polymer surfaces: morphology and charge structure. *Langmuir* **1992**, *8*, 1199−1203.
(18) Lee, L. H. Dual mechanism for metal-polymer contact electrification. *J. Electrostat.* **1994**, *32*, 1−29.
(19) Watson, P. K.; Yu, Z. Z. The contact electrification of polymers and the depth of charge penetration. *J. Electrostat.* **1997**, *40−41*, 67−72.
(20) Chandrasekar, M. S.; Pushpavanam, M. Pulse and pulse reverse plating-conceptual, advantages and applications. *Electrochim. Acta* **2008**, *53*, 3313−3322.
(21) Kelly, J. J.; Bradley, P. E.; Landolt, D. Additive effects during pulsed deposition of Cu-Co nanostrucutures. *J. Electrochem. Soc.* **2000**, *147*, 2975−2980.
(22) Kollia, C.; Loizos, Z.; Spyrellis, N. Influence of pulse reversed current technique on the crystalline orientation and surface morphology of nickel electrodeposits. *Surf. Coat. Technol.* **1991**, *45*, 155−160.
(23) Alfantazi, A. M.; Brehaut, G.; Erb, U. The effects of substrate material on the microstructure of pulse-plated Zn-Ni alloys. *Surf. Coat. Technol.* **1997**, *89*, 239−244.
(24) Fang, H.; Wu, W.; Song, J.; Wang, Z. L. Controlled growth of aligned polymer nanowires. *J. Phys. Chem. C* **2009**, *113*, 16571−16574.